ELSEVIER

Journal of Crystal Growth 220 (2000) 308–315

JOURNAL OF CRYSTAL GROWTH

www.elsevier.nl/locate/jcrysgro

Origin of domain structure in hexagonal silicon carbide boules grown by the physical vapor transport method

Seoyong Ha, Noel T. Nuhfer, Gregory S. Rohrer, Marc De Graef, Marek Skowronski*

Department of Materials Science & Engineering, Carnegie Mellon University, 5000 Forbes Avenue, Pittsburgh, PA 15213, USA

Received 1 November 1999; accepted 15 June 2000
Communicated by A.F. Witt

Abstract

Transmission electron microscopy (TEM), high-resolution X-ray diffraction, and KOH etching have been used to study the dislocation structure of 4H SiC crystals grown by the physical vapor transport method. Many of the etch pits on the Si(0 0 0 1) surface form arrays extending along the $\langle\bar{1}\,1\,0\,0\rangle$ directions. Plan view conventional and high-resolution TEM show that the arrays consist of pure edge dislocations threading along the *c*-axis with identical Burgers vectors of the $a/3\langle 1\,1\,\bar{2}\,0\rangle$ type. The dislocation arrays constitute low angle [0 0 0 1] tilt boundaries, i.e., [0 0 0 1] is the common axis lying in the boundary. Typical values of the misorientation are in the 60–200 arcsec range. Evidence is presented that such boundaries can form by polygonization of the threading edge dislocations, which have been introduced into SiC crystals by prismatic slip. © 2000 Published by Elsevier Science B.V.

PACS: 61.72.Ff

Keywords: Hexagonal SiC crystal; Physical vapor transport; Threading dislocation array; Polygonization; Prismatic slip

1. Introduction

SiC is a wide band-gap semiconductor material with unique properties making it suitable for high-power, high-temperature, and high-frequency electronic devices [1–5]. It has excellent combination of high strength, high thermal conductivity, high electric breakdown field and high saturated electron drift velocity. Recent success of the modified Lely method [6,7] in growth of large diameter bulk single crystals has spurred renewed interest in SiC based devices. However, most SiC substrates still have high densities of structural defects such as micropipes, dislocations, and low-angle grain boundaries (frequently referred to as domain walls), which will have to be reduced in order to improve the device fabrication yields. Of particular interest are extended defects propagating along the [0 0 0 1] growth direction. Such threading defects are known to penetrate active device layers deposited by epitaxy and to degrade device performance [8–12].

The existence of domains is one of the structural defects which is still not fully understood in silicon carbide boules grown along the *c*-axis by the physical vapor transport (PVT) method. Glass et al.

* Corresponding author. Tel.: +1-412-268-2710; fax: +1-412-268-3113.
E-mail address: mareks@cmu.edu (M. Skowronski).

0022-0248/00/$ - see front matter
PII: S0022-0248(00)00867-8

[13] postulated their existence on the basis of high-resolution X-ray diffraction (HRXRD) data. They observed that ω rocking curves of either symmetric or asymmetric reflections on (0 0 0 1) SiC wafers exhibit multiple peaks. Each peak had a full-width at half-maximum (FWHM) comparable to that of the single peak obtained from a high-quality Lely platelet. The number of peaks changed with the size and position of the beam footprint. Glass et al. concluded that the rocking curve structure results when the X-ray beam simultaneously diffracts from several misoriented domains. The small FWHM of the separate peaks could be explained by assuming that each domain was of high structural quality and contained few defects. The misorientation responsible for the multiple peaks was assumed to take the form of walls between domains, which have high dislocation densities. The size of domains was estimated at approximately 1 mm^2 on the wafer surface. Glass et al. proposed a model for the appearance of domains. They suggested that a SiC crystal grows by a screw dislocation mechanism with numerous independent growth centers (micropipes and screw dislocations). The initial accidental misorientations between nuclei are proposed to be settled into the crystal by the domain walls when the nuclei impinge. This interpretation was supported by Tuominen et al. [14] using KOH etching. Their micrograph of an etched (0 0 0 1) SiC wafer shows a well-defined domain structure. Centers of domains exhibit relatively few dislocation etch pits, while the domain walls have high etch pit densities. Further data were provided by Takahashi et al. [15]. They concluded, in agreement with the above authors, that domains are grown-in type with most of the defects inherited from the seed or originating at the seed–boule interface. The misorientations between domains were determined to have both a twist and a tilt components and to consist of threading edge and screw dislocations. Takahashi et al. also noticed the tendency of dislocation etch pits to line up along the $\langle \bar{1}\,1\,0\,0 \rangle$ directions.

In this work, we studied the structure of domain walls using a combination of transmission electron microscopy (TEM), HRXRD, and KOH etching. A new formation mechanism is proposed and a supporting evidence is presented.

2. Experimental procedures

The crystals used in this study were grown by Cree Research, Inc. (Durham, NC) as a part of the development program of high-temperature electronics, supported by the Defense Advanced Research Project Agency. Two inch diameter wafers were undoped or n-doped ($\sim 10^{18}\,cm^{-3}$) and oriented along (0 0 0 1) to within 0.5°. Chemical wet etching in molten KOH was used to reveal the defect structure on Si(0 0 0 1) faces of the wafers. All wafers were etched at 500°C or 510°C for 10 min. The etch pits were observed using Nomarski-contrast optical microscopy and classified with respect to their morphology. Laue X-ray diffraction was employed to determine the orientation of etch pit arrays. The specimens for TEM observations were cut from specific areas of the wafers and lapped down to a thickness of about 100 μm with boron carbide abrasive powder. They were then dimpled to a thickness of about 20 μm with 6 μm diamond paste. Finally, the samples were sputtered by Ar^+ beam in a Gatan Precision Ion Polishing System to obtain electron transparency. The TEM observations were carried out on a Philips EM420-TEM and on a JEOL 4000 EX-TEM, operated at 120 and 400 kV, respectively. HRXRD was conducted using Cu $K_{\alpha 1}$ radiation on a Philips MRD diffractometer, equipped with a four bounce monochromator and a two bounce analyzer crystal employing Ge (2 2 0) reflection. All rocking curves were obtained in triple axis mode with the analyzer crystal between a sample and the detector. The angular resolution was better than 0.004° ($\sim 14''$).

3. Results and discussion

Fig. 1 is an optical micrograph of the KOH etched Si(0 0 0 1) face of a 4H SiC wafer. Many small etch pits shown as black dots were distributed uniformly over the surface and a few large etch pits marked M could also be seen. The small and large etch pits had round and hexagonal shapes, respectively, as shown in Fig. 2, which is the magnified image of the vicinities of the two large etch pits in Fig. 1. The hexagonal etch pits were between 20 and 25 μm in size and the round etch pits had

diameters between 4 and 8 μm. According to the previous studies, we surmised that the hexagonal etch pits formed at the intersections of micropipes and the wafer surface, and the round etch pits were due to dislocations [12,14–19].

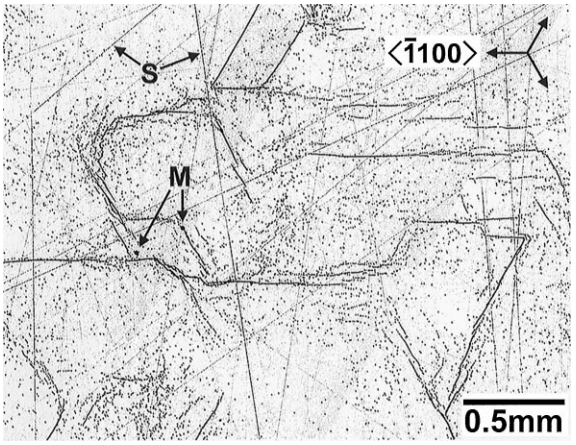

Fig. 1. Optical micrograph of the KOH etched Si(0 0 0 1) face of a 4H SiC wafer. Etched features due to scratches and micropipes are marked S and M, respectively.

Two types of linear features are visible in Fig. 1. The lines marked S have no angular relations with each other and were interpreted as due to residual mechanical damage on the surface caused by lapping and/or polishing (i.e., scratches). They will not be further considered. The second type of features are well-defined lines aligned along three different directions 60° apart from each other. The directions of the lines were of the $\langle \bar{1}\,1\,0\,0 \rangle$ type as determined by Laue X-ray diffraction. This can also be seen in Fig. 2. The line directions are perpendicular to the sides of the hexagonal etch pits, of which the directions are of the $\langle 1\,1\,\bar{2}\,0 \rangle$ type [15]. Closer inspection at high magnification (Fig. 2) reveals that the lines consist of closely spaced small etch pits. Thus, the lines are traces of dislocation arrays intersecting the wafer surface. The linear etch pit densities along the arrays were estimated to be on the order of $10^4\,cm^{-1}$, while the areal etch pit densities in areas without these arrays were on the order of $10^4\,cm^{-2}$. The corresponding average distances between neighboring dislocations are on the order of 1 μm in the arrays and 100 μm away from them. Most small etch pits in Fig. 2 appear conical in shape with a point bottom and circular outline on the

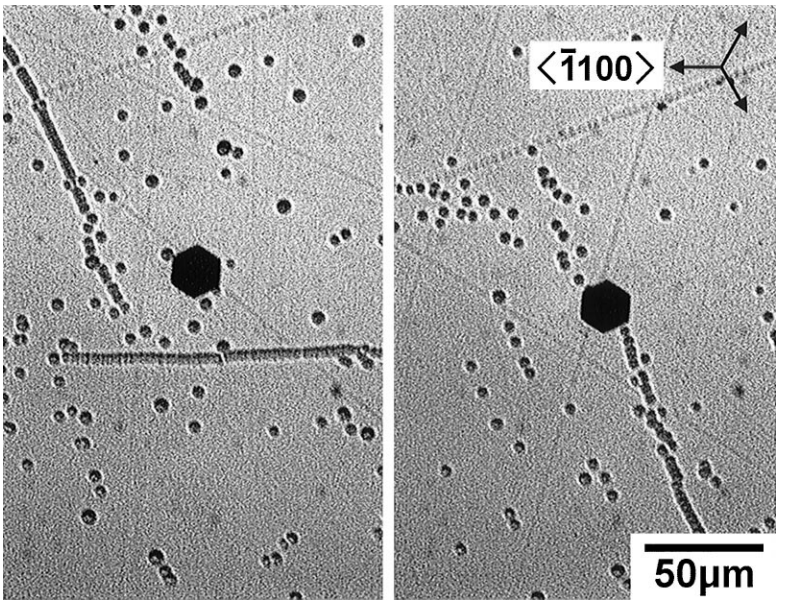

Fig. 2. Magnified optical micrographs of the two hexagonal micropipe etch pits in Fig. 1 and the small etch pit arrays. The arrays are aligned perpendicular to the sides of the hexagonal etch pits.

wafer surface. Such shape implies that the pits are due to threading dislocations extending approximately normal to the basal plane and the wafer surface. In particular, they are different from the shell etch pits assigned to basal plane dislocations by Takahashi et al. [16]. In addition, etch pits on the carbon face usually formed the mirror image of pits on the silicon face. That is, mirror imaged features of etch pits such as arrays were seen on both faces of the wafers at a same position. This observation also confirmed that the dislocations were threading along the wafer thickness. As shown in Fig. 1, the dislocation arrays frequently formed hexagonal or triangular patterns on the wafer surface, which is reminiscent of the domain wall pattern reported by Tuominen et al. [14]. In the remainder of this paper, we describe the results of TEM and HRXRD analysis of the dislocations making up the domain walls.

Fig. 3(a) is a plan view conventional TEM image showing a part of one of the arrays shown in Fig. 1. Four dislocations are visible and are marked with arrows in the figure. They form a straight line along a $\langle \bar{1}\,1\,0\,0 \rangle$ type direction. The wide white contrast features are bend contours due to changing thickness across the sample foil. This image was taken in a two beam diffraction condition with the crystal foil slightly tilted from the *c*-axis by an angle smaller than 5°. The fact that the dislocation images are nearly point-like in this projection implies that the dislocation lines are almost parallel to the *c*-axis. High-resolution TEM allowed to determine the line directions and Burgers vectors of the individual dislocations more precisely. Fig. 3(b) is a plan view high-resolution lattice image around a dislocation in the array shown in Fig. 3(a). The image was taken by choosing the *c*-axis as the zone axis. The white circular contrast represents each column of Si–C atoms perpendicular to the basal plane. The dislocation is of a pure edge type and is threading along the *c*-axis without tilt. Its core is at the intersection of the two extra half planes marked with two rows of dots. The corresponding Burgers vector, determined by drawing a Burgers circuit around the core, is of the $a/3\langle 1\,1\,\bar{2}\,0 \rangle$ type with a direction marked with an arrow. The relative orientation of the dislocation in Fig. 3(b) with respect to the array was determined by reducing the magnification in the high-resolution experiment until the image captured two dislocations in the array. Based on this observation, Fig. 3(b) could be properly oriented with respect to Fig. 3(a) while the two images were obtained in separate experiments in different microscopes. A comparison of the two images clearly demonstrates that the Burgers vector of the dislocation is perpendicular to the array direction. All the dislocations in Fig. 3(a) were determined to have identical Burgers vectors. It is further inferred here that all dislocations in an array have identical Burgers vectors. A similar

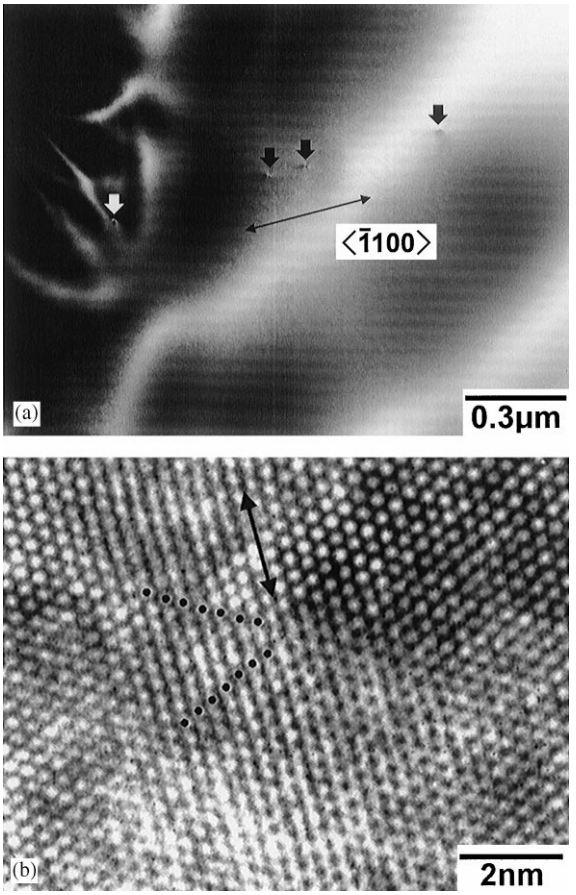

Fig. 3. (a) Plan view bright field conventional TEM micrograph showing a part of an $\langle \bar{1}\,1\,0\,0 \rangle$ dislocation array; (b) Plan view lattice image along the *c*-axis around a dislocation in the array shown in (a). The two extra half planes are marked with two rows of dots. The corresponding Burgers vector direction is indicated by an arrow.

conclusion was reached by Takahashi et al. [15] based on the contrast analysis of X-ray topography images.

The arrays of dislocations which have identical Burgers vectors perpendicular to the array direction can be viewed as low-angle grain boundaries. The average distances between neighboring dislocations in the arrays were estimated to be between 0.3 and 1 μm. These correspond to misorientation values of 60–200 arcsec across the arrays. The expected type of misorientation is pure tilt with a common rotation axis parallel to the [0 0 0 1] direction. The tilt- (or twist-) type misorientation refers to a nomenclature commonly used in polycrystalline materials. In general, when the common rotation axis of the adjacent grains is in the boundary, the misorientation is referred to as tilt. A twist misorientation corresponds to a common rotation axis perpendicular to the boundary. Low-angle twist boundaries consist of two perpendicular arrays of screw dislocations. In three-dimensional space, a general misorientation can be resolved into three independent rotation components around an arbitrary set of three orthogonal axes. The three axes for the misorientation across a boundary are usually chosen such that two of them are in the boundary and the last is perpendicular to the boundary, so as to make use of the nomenclature described above. Thus, any misorientation across a boundary can be referred to a combination of two tilt and a twist components. For the case considered here, since the boundaries are perpendicular to the (0 0 0 1) plane of hexagonal SiC, we selected one of the two in-boundary tilt axes as the *c*-axis.

Our conclusion regarding the character of the misorientation across the observed dislocation arrays is a consequence of the assumption that all dislocations in the array are identical. Since the TEM technique is limited to small sample sizes, it would be very difficult to test this assumption by direct observation. Instead, we employed high-resolution X-ray diffraction. Fig. 4 shows the etch pit distribution on the Si(0 0 0 1) face of one of the samples selected for this experiment. The sample was of rectangular shape with two parallel side walls formed by cleaving along a $\{\bar{1}\,1\,0\,0\}$ type plane. One of these facets is shown in the upper

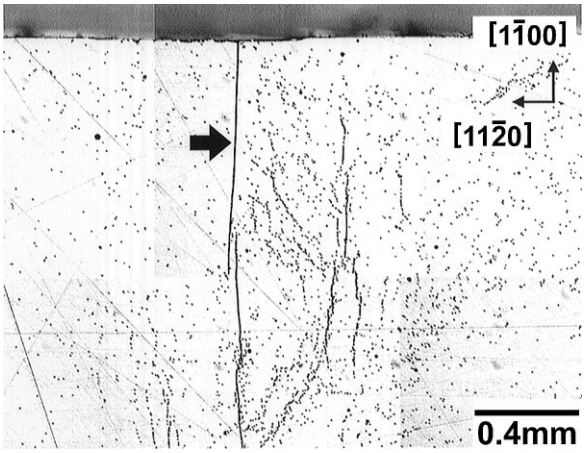

Fig. 4. Optical micrograph of a sample used for HRXRD experiments. One well-defined $\langle\bar{1}\,1\,0\,0\rangle$-oriented dislocation array is visible and perpendicular to the cleaved $(1\,\bar{1}\,0\,0)$ sample face shown in the upper part of the figure.

portion of Fig. 4. The sample was cleaved from a wafer region with a low density of the dislocation arrays. Only one well-defined array is visible in the 4 mm × 4 mm sample area, intersecting the cleaved side facet.

Fig. 5(a)–(c) are the three HRXRD ω rocking curves collected in three different orientations of the diffraction plane with respect to the array in Fig. 4. Each orientation gives one of the three components of the total misorientation, more specifically the rotation around the diffraction plane normal. The experimental configurations and the corresponding misorientation components for each case are illustrated in Fig. 6. The curve shown in Fig. 5(a) was obtained with the diffraction plane normal in the basal plane ((0 0 0 8) reflection was used) and parallel to the array direction. For Fig. 5(b), the diffraction plane normal was in the basal plane and perpendicular to the array direction. These two measurements determined the misorientation of the basal plane. The former is one of the two tilt components of the low-angle boundary and the latter is the twist component. The second tilt component was measured using the $(\bar{1}\,1\,0\,0)$ reflection with the sample mounted on the side facet. In this orientation, the diffraction plane normal was parallel to the crystal *c*-axis. The size of the beam footprint on the sample was 0.6 mm width

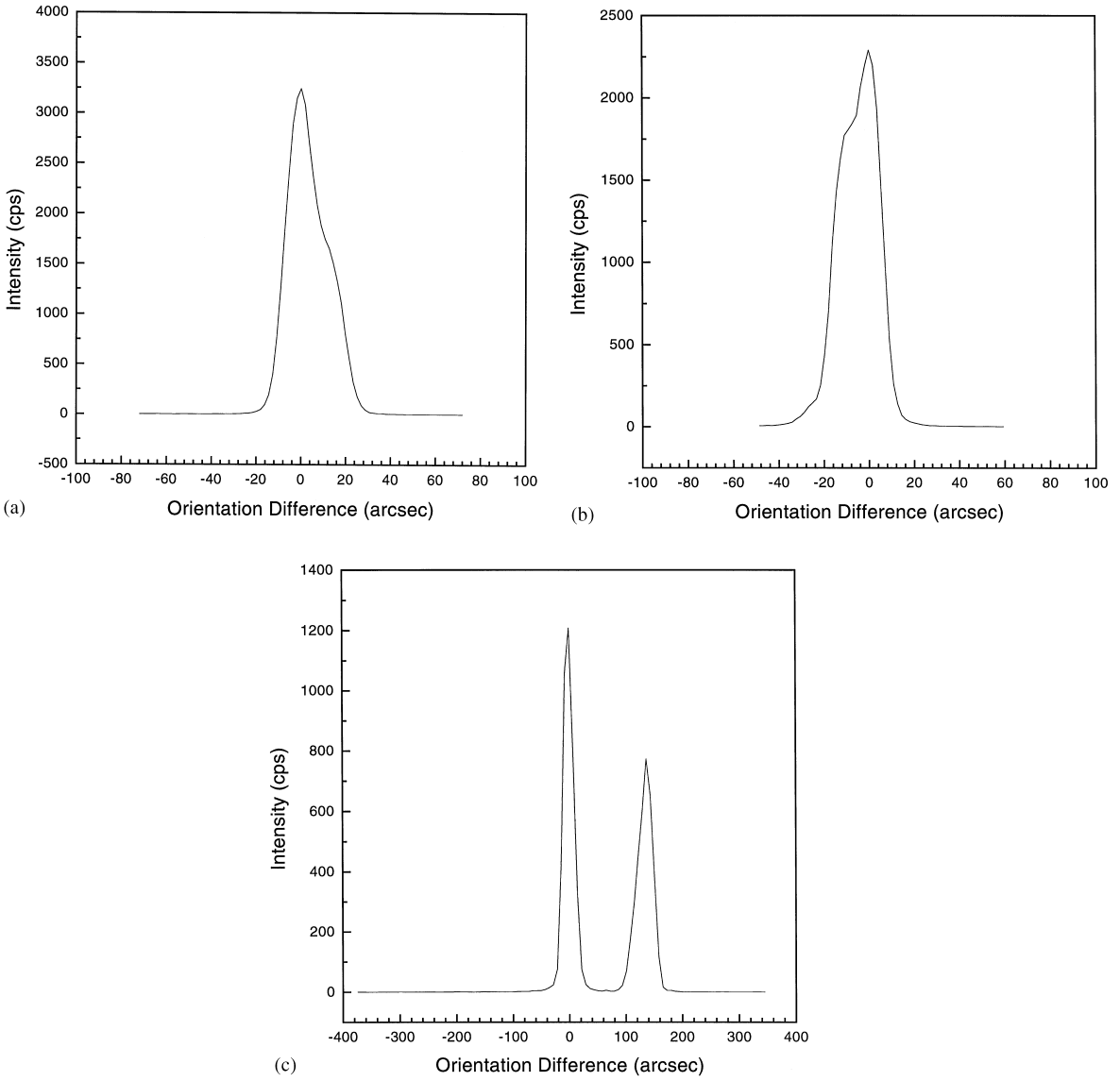

Fig. 5. ω rocking curves obtained from the array in Fig. 4 in three experimental configurations. (a) diffraction plane normal in the basal plane, parallel to the array; (b) diffraction plane normal in the basal plane, perpendicular to the array; (c) diffraction plane normal parallel to the c-axis.

$\times$ 3.5 mm height for the (0 0 0 8) reflection and 1.6 mm $\times$ 3.5 mm for the ($\bar{1}$ 1 0 0) reflection. In the first two configurations (Fig. 5(a) and (b)), the resulting ω rocking curves consist of a single diffraction peak with FWHM of 30 arcsec. A trace of fine structure is visible in the form of a single shoulder in each curve. The separation of the shoulder from the dominant peak in either case was below 10 arcsec. The rocking curve in Fig. 5(c) shows two well-defined peaks separated by about 140 arcsec. The two peaks are due to reflections from two misoriented domains delineated by etching. These

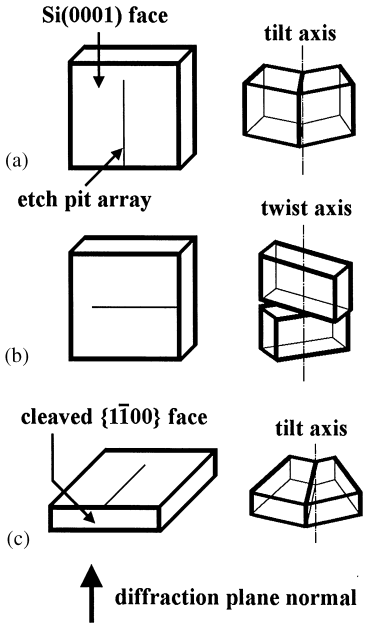

Fig. 6. The relationship between experimental configuration and the corresponding misorientation component for each case (a), (b), and (c) in Fig. 5. The crystal *c*-axis is perpendicular to the Si(0 0 0 1) face (the largest face) for each case in the left column of specimen configurations.

HRXRD results agree very well with the model of the dislocation arrays presented above. Thus, the low-angle grain boundaries shown in Fig. 1 are almost pure tilt-type corresponding to rotations around the *c*-axis. The domain walls are made of pure edge threading dislocations with Burgers vectors of the $a/3\langle 1\,1\,\bar{2}\,0\rangle$ type.

It is worth noting that the above interpretation of the domain wall structure cannot result in the misorientations that can be detected by (0 0 0 n)-type reflection. On the other hand, many authors reported multiple peaks present in such reflections and we have observed them also at selected locations on some wafers. This implies that, in addition to the domains described above, there is a second type of domain with different morphology and probably a different origin. More detailed experiments are needed in order to elucidate this aspect of SiC structure.

The remaining question is the mechanism responsible for formation of the threading dislocation arrays and domain structure described in this report. In a recent paper, we have reported clear experimental evidences of activation of the secondary slip system in hexagonal silicon carbide crystals grown by the PVT method [20]. The slip was of $a/3\langle 1\,1\,\bar{2}\,0\rangle\{\bar{1}\,1\,0\,0\}$ type and produced dislocations with line direction along the *c*-axis. The apparent source of stress was the difference of thermal expansion between the matrix boule and either the misoriented grains or polytypic inclusions at periphery of SiC crystals. In either case, the secondary slip dislocations were introduced during post-growth cooling and formed easily recognizable slip band patterns on basal plane cut wafers. The slip bands were typically 100 μm wide and 10 mm long, originated at the misoriented grains or polytypic inclusions, and were oriented along the $\langle 1\,1\,\bar{2}\,0\rangle$ directions. In some cases, the slip bands almost reached the center of the crystals.

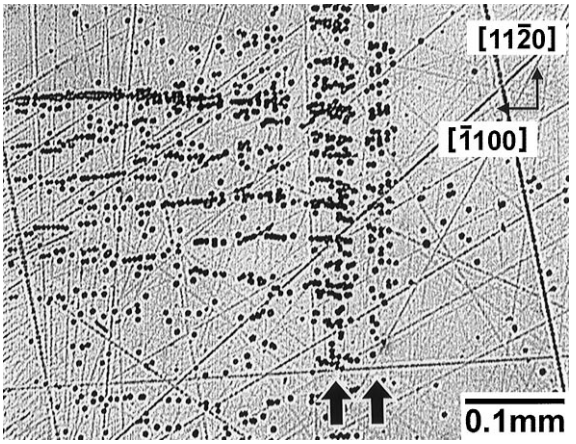

Fig. 7. Optical micrograph of the detail of two slip bands showing partial polygonization.

Fig. 7 is an optical micrograph showing the detail of two slip bands. The slip bands extended vertically and are marked with arrows. It is clear that etch pit distribution within a slip band shows a fine structure consisting of many small fragmentary arrays aligned in the direction perpendicular to that of the slip band. Since the Burgers vectors of the dislocations within a slip band are identical and parallel to the slip direction, they must be perpendicular to the fragment direction. It is plausible to

suggest that the fragmentary alignment occurred in order to lower the energy of the system. It is well known that the low-energy configuration for an array of edge dislocations corresponds to an array in which Burgers vectors are perpendicular to the array direction [21]. This leads to the overlap of tensile and compressive stress regions around neighboring dislocations and a reduction of the total strain energy. The process of alignment is referred to as polygonization. Fig. 7 shows an initial stage of polygonization of the threading edge dislocations in the slip bands. The process occurred either during post-growth cooling or during any post-growth high-temperature annealing. It is easy to visualize that if this wafer was subsequently used as a seed in the PVT growth process, the significantly high growth temperature and long time would allow the polygonization to complete. Through glide and/or climb, dislocations introduced by slip could align themselves into the pattern shown in Fig. 1. Thus, the domain structure of pure tilt boundaries studied in this work would be due to plastic deformation of the already solidified crystal followed by dislocation polygonization.

4. Summary

Threading dislocations forming etch pit arrays along $\langle \bar{1}100 \rangle$ directions were revealed by KOH etching on Si(0001) faces of [0001] grown 4H SiC crystals. Conventional and high-resolution TEM have identified pure edge dislocations lying along the *c*-axis with Burgers vectors of the $a/3\langle 11\bar{2}0 \rangle$ type. The Burgers vectors of the individual dislocations in an array were identical and perpendicular to the array direction. The misorientations across the arrays were estimated to be in the 60–200 arcsec range. The type of misorientation was identified as a pure tilt corresponding to the rotation around a common axis parallel to the *c*-axis. Based on the distribution of dislocations in secondary slip bands, the arrays were interpreted as formed by polygonization of the threading edge dislocations.

Acknowledgements

This work was supported in part by the Commonwealth of Pennsylvania through the Ben Franklin Technology Center (Grant No. 98W.CM00562R-1) and by National Science Foundation (Grant No. DMR.9903702). We would like to thank to Dr. W.C. Mitchel of the Air Force Research Laboratory for his providing the SiC wafers.

References

[1] M. Bhatnagar, B.J. Baliga, IEEE Trans. Electron Dev. 40 (1993) 645.
[2] T.P. Chow, M. Ghezzo, MRS Symp. Proc. 423 (1996) 9.
[3] C.E. Weitzel, K.E. Moore, MRS Symp. Proc. 483 (1998) 111.
[4] B.J. Baliga, MRS Symp. Proc. 512 (1998) 77.
[5] C.E. Weitzel, Mater. Sci. Forum 264–268 (1998) 907.
[6] Y.M. Tairov, V.F. Tsvetkov, J. Crystal Growth 43 (1978) 209.
[7] Y.M. Tairov, V.F. Tsvetkov, J. Crystal Growth 52 (1981) 146.
[8] P.G. Neudeck, J.A. Powell, IEEE Electron Dev. Lett. 15 (1994) 63.
[9] G. Gradinaru, M. Helmi, Y. Khlebnikov, G. Korony, W.C. Mitchel, T.S. Sudarchan, MRS Symp. Proc. 442 (1997) 643.
[10] U. Zimmermann, A. Hallén, A.O. Konstantinov, B. Breitholtz, MRS Symp. Proc. 512 (1998) 151.
[11] P.G. Neudeck, W. Huang, M. Dudley, IEEE Trans. Electron Dev. 46 (1999) 478.
[12] K. Koga, Y. Fujikawa, Y. Ueda, T. Yamaguchi, Amorphous and Crystalline Silicon Carbide IV, Proceedings in Physics, Vol. 71, Springer, Berlin, 1992, p. 96.
[13] R.C. Glass, L.O. Kjellberg, V.F. Tsvetkov, J.E. Sundgren, E. Janzén, J. Crystal Growth 132 (1993) 504.
[14] M. Tuominen, R. Yakimova, R.C. Glass, T. Tuomi, E. Janzén, J. Crystal Growth 144 (1994) 267.
[15] J. Takahashi, N. Ohtani, M. Kanaya, J. Crystal Growth 167 (1996) 596.
[16] J. Takahashi, M. Kanaya, Y. Fujiwara, J. Crystal Growth 135 (1994) 61.
[17] J. Takahashi, N. Ohtani, Phys. Stat. Sol. B 202 (1997) 163.
[18] N. Sugiyama, A. Okamoto, K. Okumura, T. Tani, N. Kamiya, J. Crystal Growth 191 (1998) 84.
[19] N. Ohtani, J. Takahashi, M. Katsuno, H. Yashiro, M. Kanaya, MRS Symp. Proc. 510 (1998) 37.
[20] S. Ha, N.T. Nuhfer, G.S. Rohrer, M. De Graef, M. Skowronski, J. Electron. Mater. 29/7 (2000) L5.
[21] R.E. Reed-Hill, R. Abbaschian, in: Physical Metallurgy Principles, 3rd edition, PWS Publishing Company, Boston, USA, 1994, pp. 233–239.